age. Indeed, the methane sorption isotherm was measured in the pressure range 0 to 42 atm and room temperature and was found to have an uptake of 240 cm^3 at standard temperature and pressure (STP)/g [155 cm^3 (STP)/cm^3] at 298 K and 36 atm (Fig. 3C). This exceeds that of other crystalline materials including zeolite 5A (87 cm^3/cm^3) and other coordination frameworks [up to 213 cm^3 (STP)/g] (17, 20, 21). On the basis of volume for volume (v/v), the amount of methane sorbed by IRMOF-6 at 36 atm (which is regarded as a safe and cost-effective pressure limit) represents 70% of the amount stored in compressed methane cylinders in laboratories where much higher, unsafe levels of pressure (205 atm) are used. Reducing the pressure represents an advance that we believe will affect the future use of these materials in automobile fueling (22).

Methane uptake was also evaluated by testing IRMOF-1 and IRMOF-3 under the same conditions where their uptake was found to be lower [135 and 120 cm^3 (STP)/cm^3] than that of IRMOF-6—a significant difference that is attributable to the hydrophobic nature of C_2H_4 units in IRMOF-6. Thus, functionalizing the pores with larger hydrocarbons as illustrated in IRMOF-4, -5, and -7, may indeed result in even higher capacities. The most open members of this series (IRMOF-12 and -14) are also porous, in that they exhibit behavior similar to that described for IRMOF-6. In addition, they maintain their crystallinity in the absence of guests, as demonstrated by the coincidence of the XRD patterns of the synthesized material with those measured for the evacuated form of IRMOF-12 and -14.

The intrinsic value of this design approach lies in the ability to control and direct the reticulation of building blocks into extended networks in which specific properties can be targeted.

References and Notes
1. A. Stein *et al.*, *Science* **259**, 1558 (1993).
2. P. J. Fagan, M. D. Ward, *Sci. Am.* **267**, 48 (1992).
3. O. M. Yaghi *et al.*, *J. Solid State Chem.* **152**, 1 (2000).
4. M. Eddaoudi *et al.*, *Acc. Chem. Res.* **34**, 319 (2001).
5. V. A. Russell *et al.*, *Science* **276**, 575 (1997).
6. Y. H. Kiang *et al.*, *J. Am. Chem. Soc.* **121**, 8204 (1999).
7. B. F. Hoskins, R. Robson, *J. Am. Chem. Soc.* **111**, 5962 (1989).
8. F. Serpaggi, G. Férey, *J. Mater. Chem.* **8**, 2749 (1998).
9. H. Li *et al.*, *Nature* **402**, 276 (1999).
10. "Reticular" is an adjective, defined in Random House Webster Unabridged Dictionary as "having the form of a net; netlike." Isoreticular is defined as "having the same network topology."
11. All IRMOFs were formulated as $Zn_4O(Link)_3(DEF)_x$. [See (23) for details of elemental analyses.]
12. All the intensity data were collected on Bruker SMART CCD diffractometer with a graphite mono-chromated MoKα (λ = 0.71073 Å) radiation. Structures were solved by direct methods, and successive difference Fourier syntheses with SHELXTL software package. Final $R1$ values were calculated with $I > 2\sigma(I)$. Crystal data are as follows: IRMOF-2, cubic, space group *Fm-3m*, a = 25.772(1) Å, V = 17117(1) Å^3, Z = 8, R1 = 0.0976; IRMOF-3, cubic, *Fm-3m*, a = 25.747(1) Å, V = 17067(2) Å^3, Z = 8, R1 = 0.1160;

IRMOF-4, cubic, *Fm-3m*, a = 25.849(1) Å, V = 17272(2) Å^3, Z = 8, R1 = 0.0706; IRMOF-5, cubic, *Pm-3m*, a = 12.882(1) Å, V = 2137.6(3) Å^3, Z = 1, R1 = 0.1181; IRMOF-6, cubic, *Fm-3m*, a = 25.842(2) Å, V = 17258(2) Å^3, Z = 8, R1 = 0.1325; IRMOF-7, cubic, *Pm-3m*, a = 12.914(3) Å, V = 2153.9(7) Å^3, Z = 1, R1 = 0.1957; IRMOF-8, cubic, *Fm-3m*, a = 30.092(2) Å, V = 27248(3) Å^3, Z = 8, R1 = 0.1691; IRMOF-9, orthorhombic, *Pnnm*, a = 17.147(1) Å, b = 23.322(1) Å, c = 25.255(1) Å, V = 10099.6(8) Å^3, Z = 4, R1 = 0.0802; IRMOF-10, [single crystals of sufficient quality to perform a single-crystal analysis study could not be obtained, but its observed x-ray powder diffraction pattern was the same as that observed for IRMOF-12 (below) and was confirmed by a simulated pattern for IRMOF-10 based on IRMOF-12 coordinates] cubic, *Fm-3m*, a = 34.281(2) Å, V = 40286(4) Å^3, Z = 8; IRMOF-11, trigonal, *R-3m*, a = 24.822(1) Å, c = 56.734(3) Å, V = 30272(3) Å^3, Z = 12, R1 = 0.0963; IRMOF-12, cubic, *Fm-3m*, a = 34.281(2) Å, V = 40286(4) Å^3, Z = 8, R1 = 0.1080; IRMOF-13, (same as treatment for IRMOF-10 but with the use of IRMOF-11) trigonal, *R-3m*, a = 24.822(1) Å, c = 56.734(3) Å, V = 30272(3) Å^3, Z = 12; IRMOF-14, cubic, *Fm-3m*, a = 34.381(13) Å, V = 40642(26) Å^3, R1 = 0.1914; IRMOF-15, cubic, *Im-3m*, a = 21.459(1) Å, V = 9882(1) Å^3, Z = 1, R1 = 0.1164; IRMOF-16, cubic, *Pm-3m*, a = 21.490(1) Å, V = 9925(1) Å^3, Z = 1, R1 = 0.1845. [See (23) for details.]
13. M. O'Keeffe, B. G. Hyde, *Crystal Structures I: Patterns and Symmetry* (Mineralogy Society of America, Washington, DC, 1996).
14. T. M. Reineke *et al.*, *J. Am. Chem. Soc.* **122**, 4843 (2000).
15. M. J. Bennett, J. V. Smith, *Mater. Res. Bull.* **3**, 633 (1968).
16. N. Hüsing, U. Schubert, *Angew. Chem. Int. Ed.* **37**, 22 (1998).
17. V. C. Menon, S. Komarneni, *J. Porous Mater.* **5**, 43 (1998).
18. A van der Waals radius of C (1.70 Å) was used in determination of distance parameters [A. Bondi, *J. Phys. Chem.* **68**, 441 (1964)].
19. M. Eddaoudi *et al.*, *J. Am. Chem. Soc.* **122**, 1391 (2000).
20. K. Seki, *Chem. Commun.* **16**, 1496 (2001).
21. S. Noro *et al.*, *Angew. Chem. Int. Ed.*, **39**, 2081 (2000).
22. K. Seki *et al.*, U.S. patent 5,862,796 (1999).
23. Single crystal XRD data and elemental microanalyses for IRMOF-2 through -16, including sorption and XRD data for IRMOF-12 and -14, are available as supplementary material on *Science* Online at www.sciencemag.org/cgi/content/full/295/5554/469/DC1.
24. Supported by NSF (M.O., O.M.Y.) and DOE (O.M.Y.). We thank D. Martin (University of Michigan, Material Sciences Engineering) for supplying a sample of the free R_6-BDC acid.

11 October 2001; accepted 6 December 2001

Spider Silk Fibers Spun from Soluble Recombinant Silk Produced in Mammalian Cells

Anthoula Lazaris,[1]* **Steven Arcidiacono,**[2] **Yue Huang,**[1] **Jiang-Feng Zhou,**[1] **François Duguay,**[1] **Nathalie Chretien,**[1] **Elizabeth A. Welsh,**[2] **Jason W. Soares,**[2] **Costas N. Karatzas**[1]

Spider silks are protein-based "biopolymer" filaments or threads secreted by specialized epithelial cells as concentrated soluble precursors of highly repetitive primary sequences. Spider dragline silk is a flexible, lightweight fiber of extraordinary strength and toughness comparable to that of synthetic high-performance fibers. We sought to "biomimic" the process of spider silk production by expressing in mammalian cells the dragline silk genes (*ADF-3/MaSpII* and *MaSpI*) of two spider species. We produced soluble recombinant (rc)−dragline silk proteins with molecular masses of 60 to 140 kilodaltons. We demonstrated the wet spinning of silk monofilaments spun from a concentrated aqueous solution of soluble rc−spider silk protein (ADF-3; 60 kilodaltons) under modest shear and coagulation conditions. The spun fibers were water insoluble with a fine diameter (10 to 40 micrometers) and exhibited toughness and modulus values comparable to those of native dragline silks but with lower tenacity. Dope solutions with rc−silk protein concentrations >20% and postspinning draw were necessary to achieve improved mechanical properties of the spun fibers. Fiber properties correlated with finer fiber diameter and increased birefringence.

The evolutionary survival of spiders has been tightly linked to the diversity, production, and use of silks (1–3). Orb-web spinning spiders have as many as seven highly specialized

glands, each producing silk with different mechanical properties and functions (4–6). Dragline silk, used as the safety line and as the frame thread of the spider's web, is one of the strongest silks studied, being three times as tough as aramid fibers and five times stronger by weight than steel (7–10).

The protein core of dragline silk fibers is secreted as a mixture of two soluble proteins from specialized columnar epithelial cells of the major ampullate gland of orb-weaver

[1]Nexia Biotechnologies, Vaudreuil-Dorion, Quebec J7V 8P5, Canada. [2]Materials Science Team, U.S. Army Soldier Biological Chemical Command, Natick, MA 01760, USA.

*To whom correspondence should be addressed. E-mail: alazaris@nexiabiotech.com

spinning spiders (*1*, *7*). Partial cDNA clones encoding the two protein components of dragline silk have been isolated and characterized from two species of orb-web weaving spiders (*Araneus diadematus*: ADF-3 and ADF4; and *Nephila clavipes*: MaSpI and MaSpII) (*11–13*).

Dragline silk genes encode proteins that contain iterated peptide motifs (*14*) exhibiting a pattern of alternating Ala-rich, crystal-forming blocks (ASAAAAAA blocks) that impart the silk's mechanical properties (*14–16*) and Gly-rich amorphous blocks [GGYGPG, (GPGQQ)$_n$], implicated in providing elasticity in the silk filament (*17*). The process by which spiders spin soluble silk protein into strong, liquid-crystal fibers is a product of 400 million years of evolution. Silk fibers begin to form within the spiders' silk gland from an acidified liquid crystalline-form solution (protein concentration of 30 to 50%) using very small forces followed by drawing in the air after the fiber has left the spiders' body (*7*). The unique mechanical properties of the spider silk filaments and an inability to domesticate spiders have driven numerous attempts to artificially manufacture spider dragline silks for industrial and medical applications. Recombinant (rc)–spider silk proteins have been produced in bacteria and yeast systems with limited success (*18–22*). The highly repetitive structure and the unusual mRNA secondary structure result in inefficient translation that limits the size of the silks produced (*23*). The feasibility of producing soluble rc–spider silks (up to 100 kD) by using synthetic genes (*MaSpI*) in transgenic plants has been reported recently (*24*). Several groups have attempted to spin silk protein fibers artificially. Most efforts have involved wet spinning of reconstituted *Bombyx mori* (*25–27*) or native spider silk (*28*, *29*). Recombinant silk proteins have been spun with harsh solvents such as hexafluoroisopropanol (*30*) as diluents or dilute protein solutions in concentrated formic acid (*21*). However, the mechanical properties of the native spider silks have not been reproduced with either reconstituted or rc–spider silk proteins (*23*, *31*).

Truncated synthesis has been a limiting factor in expressing silks of high molecular weight in *Escherichia coli* and *Pichia* (*23*). To investigate whether mammalian cell systems can efficiently overcome this limitation, we generated two series of constructs for expression of rc–spider silk proteins in mammalian cells using spider dragline silk gene cDNAs: the MaSpI or MaSpII cDNAs (*12*) and the ADF-3 cDNA (*11*, *32*) (Fig. 1). In addition, expression vectors were generated containing multimers of the dragline cDNAs [ADF-33, ADF-333, and MaSpI(2)] (*32*) (Fig. 1) to produce genes that encode proteins of similar size to those found in the spider major ampullate silk gland (*23*).

Two cell lines, bovine mammary epithelial alveolar cells immortalized with large T (MAC-T) and baby hamster kidney (BHK) cells, were chosen as expression systems (*32*). Analysis of media from stable transfectants of ADF-3, MaSpI, and MaSpII constructs by Western blot (*32*) revealed prominent immunoreactive bands of the expected molecular size (Fig. 2A, lanes 1, 2, and 5; Fig. 2B, lane 1). To explore the relation between spider silk protein size and mechanical properties of spun fibers, we first evaluated the ability of the mammalian epithelial cells to produce rc–spider silk proteins of high molecular weight similar to that of silk proteins observed in the spider's silk glands (*23*). Analysis of conditioned media revealed the presence of rc–spider silk proteins of the predicted sizes (~110 and ~140 kD) (Fig. 2A, lanes 3 and 4; Fig. 2B, lane 2) produced from concatemers of the *ADF-3* gene (ADF-33 and ADF-333) and a dimer of MaSpI, respectively. In all instances, the different expression vectors used enabled the secretion of soluble silk proteins in the media. Distinct spider silk proteins with molecular sizes of 120, 150, 190, 250, and 750 kD have been found in the ampullate gland of *N. clavipes* (*23*).

Expression of the secreted 110- and 140-kD spider silk proteins from BHK cells was much lower than that of the 60-kD monomer. This may be attributed to inefficient transcription due to the high secondary structure, insufficient secretion of the larger proteins, low copy numbers of the construct being transfected, or limitations of the cell translational machinery. During silk synthesis, the spider produces gland-specific pools of tRNAs for glycine and alanine to meet the increased demand for limiting amino acids (*33*). Given the unique amino acid composition of the silk proteins (e.g., MaSpII: 32% glycine, 16% alanine), it is possible that the aminoacyl-tRNA pools of the epithelial cells grown in vitro are depleted.

ADF-3 His and ADF-3 rc–spider silk protein (25 to 50 mg/liter each; corresponding to ~20 μg per 10^6 cells per day) were produced in BHK cells with more than 12 g of material purified from conditioned culture media (*32*). The age of the hollow fiber reactor (~3 months) correlated with the appearance of lower molecular weight spider silk proteins. The appearance of this protein "ladder" was probably due to termination errors of protein synthesis. Translational pausing, resulting in heterogeneous protein expression, has been reported in *N. clavipes* (*16*, *22*) and *B. mori* (*34*).

ADF-3 was recovered from conditioned culture media by precipitation with 15 to 20% ammonium sulfate for an enrichment of at least 50% in a single step (*32*). The precipitated proteins, containing ADF-3, were readily redissolved in phosphate-buffered saline. In contrast, rc–spider silks produced in *E. coli* or yeast and precipitated similarly could only be redissolved in strong denaturing solvents such as hexafluoroisopropanol or guanidine hydrochloride (*23*). This difference in solubility may be attributed to the presence of the COOH-terminus in ADF-3 and MaSpII rc–spider silk proteins produced in mammalian cells, suggesting that the more hydrophilic COOH-terminal 100 amino acids [ab-
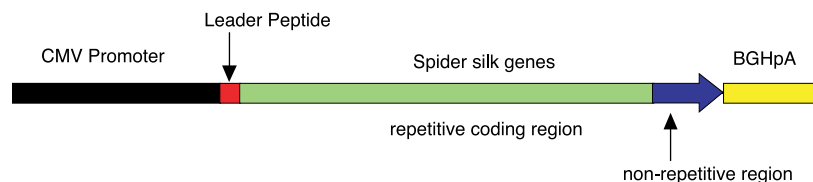
Spider Silk Genes Expressed	cDNA size (kb)	Non-repetitive 3'-end (kb)	"TAG"	Predicted rc-spider silk size	
				# amino acids	kD
ADF-3 His	1.7	0.3	Myc, His(8)	677	63
ADF-3	1.7	"		652	60
ADF-33	3.4	"		1090	110
ADF-333	4.7	"		1568	140
MaSpII	1.6	"		656	59
MaSpI	1.9	"		719	59
MaSpI(2)	3.6	"		1316	106

Fig. 1. DNA expression constructs used to produce rc–dragline spider silks in mammalian cells.
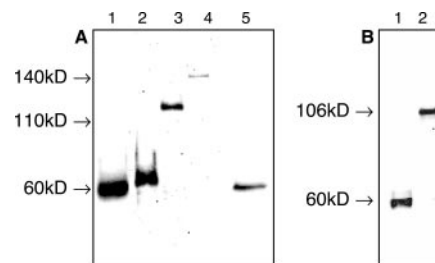

Fig. 2. Western blot analysis of media from BHK cells transfected with DNA expression constructs containing (**A**) ADF-3 and MaSpII and (**B**) MaSpI. About 20 μl of conditioned media was loaded per lane. (A) Lane 1, ADF-3 His; lane 2, ADF-3; lane 3, ADF-33; lane 4, ADF-333; lane 5, MaSpII. (B) Lane 1, MaSpI; lane 2, MaSpI (2).

sent in other studies (*23*)] may increase the solubility of the secreted silks.

Purified ADF-3 migrated as a major band with an apparent molecular mass of 60 kD on silver-stained SDS–polyacrylamide gel electrophoresis (PAGE) gels under reducing conditions (Fig. 3A, lane 4) and was recognized by ADF–specific antibodies (Fig. 3B, lane 3). The purity of rc–spider silk ranged from 80 to 90% (*32*).

The identity of the purified ADF-3 protein was further confirmed by NH_2-terminal sequencing. It exhibited identity to the first six residues of ADF-3, confirming the predicted sequence and the faithful cleavage of the leader peptide at the expected site. Amino acid analysis further confirmed the identity and purity of the ADF-3 protein (*32*).

Fiber formation, appearance, and properties depended at least in part on spin dope concentration, purity, and coagulation bath composition. ADF-3 His fibers, derived from rc–spider silk protein purified from MAC-T and BHK cells, were spun from spin dopes at concentrations of 2.8 to 8.3% (w/v) rc–silk protein and 70 to 80% purity (*35*). Water-insoluble fibers were obtained with diameters of 8 to 23 μm. Because the produced fibers were brittle and difficult to manipulate, we focused on optimizing spinning processes using ADF-3 rc–spider silk protein.

Fibers derived from ADF-3 rc–spider silk protein purified from BHK cells were spun from spin dopes at protein concentrations of 10 to 28% (w/v) and protein purity ranging from 80 to 90% (*35*). Fibers with measurable mechanical properties were obtained with spin dope rc–silk protein concentrations >10%. However, the highest tensile proper-

ties were achieved at concentrations >23%. In these experiments, the water concentration in the coagulation bath was at least 20%. The diameters of as-spun fibers averaged 40 μm. The maximum postspinning draw achieved was up to five times the fiber's original length, and the average fiber diameter decreased to 20 μm. It was necessary to constrain the fiber ends while they were being drawn and air-dried, otherwise the fiber length would shorten partially relative to the drawn length, similar to a viscoelastic material. When the fibers were completely dry, further draw was no longer possible.

Immediately after spinning, fibers were subjected to either single or double draw. Single-drawn fibers were subjected to draw in 70 to 80% methanol (Table 1) (*32*). Double-drawn fibers were drawn in methanol and then further drawn in water. Fibers subjected to higher draw ratios displayed greater toughness, tenacity, and modulus values, suggesting the importance of a high draw ratio. Improvements in all three measurements were significant when the draw ratio increased from 3 to 5 (Fig. 4, A to C). Although tenacity values increased with increased draw, no difference was observed when fibers were subjected to single or double draw at a draw ratio > 3 (Fig. 4A). The average tenacity values improved from 0.026 to 1.65 grams per denier (gpd) with a draw ratio of 5, with a concomitant decrease of the fiber diameter. The highest tenacity value obtained for ADF-3 was 2.26 gpd (Table 1). This is lower than the reported values for dragline silk (7 to 11 gpd) (Table 1) (*16*, *29*), yet similar to those measured for fibers spun from regenerated spider silk (*29*). Figure 5 represents typ-

ical stress/strain curves obtained from testing of ADF-3–based fibers (sample 1, Table 1). The maximum average toughness obtained from fibers drawn in 75% methanol was 0.645 gpd (Table 1). The highest average toughness value obtained for double-drawn ADF-3 fibers was 0.895 (Table 1) (*32*), with peak toughness measured as high as 1.60 gpd (Fig. 5). The highest average modulus obtained was 110.6 gpd, with a maximum modulus of 173 gpd recorded. These properties compared favorably with the toughness and modulus measured for native *A. diadematus* dragline silk (Table 1) (*16*, *29*).

The improved mechanical properties with postspinning draw of the rc-silk fibers agree with values reported for respun *B. mori* (*27*) and *N. clavipes* silks (*29*). In these studies, additional draw resulted in higher toughness and tenacity values. In our studies, the selection of solvent for draw was important; the mechanical properties of double-drawn fibers were superior to those of single-drawn fibers, presumably because of increased molecular orientation. Water can plasticize silks and stabilize the postspinning drawing process by packing and folding of the poly(alanine) do-

Fig. 3. Purification of ADF-3 rc–spider silk secreted from mammalian cells. (**A**) Silver-stained SDS-PAGE gel. Lane 1, molecular size markers (kD); lane 2, solubilized proteins after ammonium sulfate precipitation of BHK conditioned media loaded onto an anion-exchange column; lane 3, flow-through protein fraction from anion-exchange column; lane 4, elution fraction of bound proteins from anion-exchange column. (**B**) Western blot analysis. Lanes 1 to 3: same as lanes 2 to 4 in (A).

Fig. 4. Effect of postspinning draw on (**A**) tenacity, (**B**) toughness, and (**C**) modulus of ADF-3 rc–spider silk filaments. A fourfold draw improved both the tenacity and toughness of spun fibers for single- and double-drawn fibers. At a fivefold draw, the double-drawn fibers showed marked improvement in toughness. Double-drawn fibers with a fivefold draw have a higher modulus. In single-drawn fibers, the modulus levels off after a threefold draw.
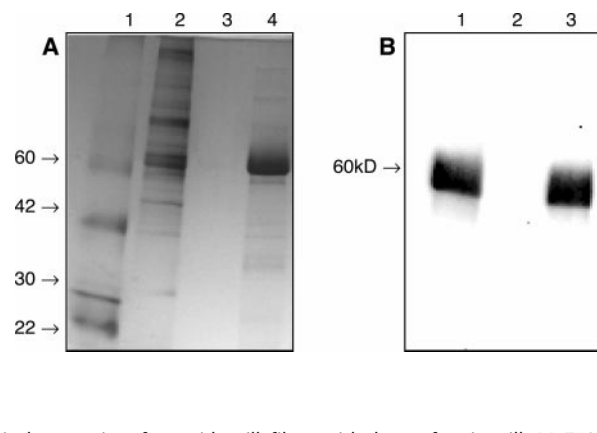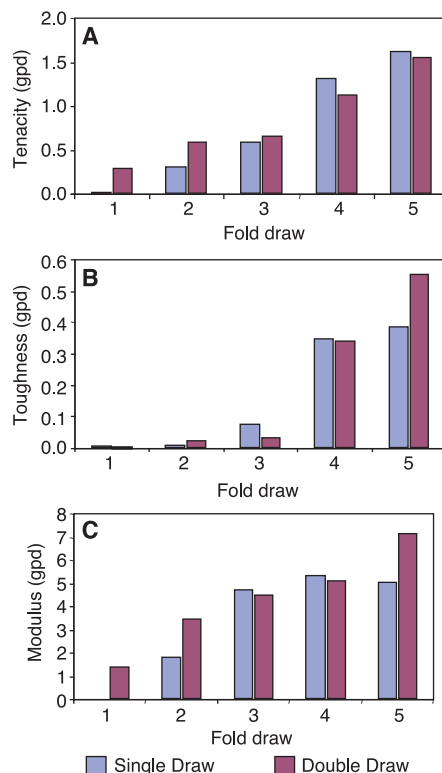
Table 1. Comparison of the mechanical properties of rc–spider silk fibers with those of native silk. M, 75% methanol; W, water; NA, not applicable.

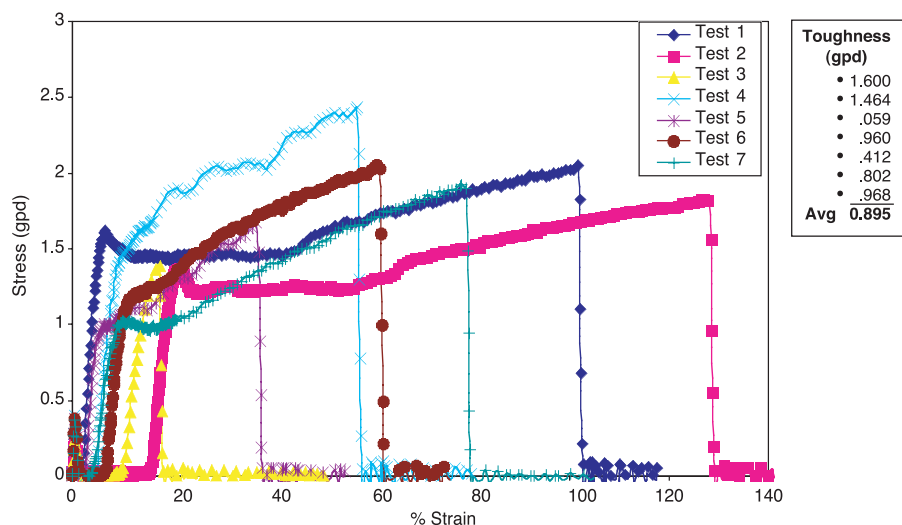| Sample	Draw	Draw ratio	Toughness (gpd)	Modulus (gpd)	% Strain break	Tenacity (gpd)	n
ADF-3, sample 1	M/W	5	0.895	42.8	59.6	1.91	7
ADF-3, sample-2	M/W	5	0.850	110.6	43.4	2.26	7
ADF-3, sample-3	M	4	0.645	63.2	45.0	1.8	5
Araneus, dragline	NA	NA	0.6–1.3	38–76	19–30	7–11	20

Fig. 5. Stress-strain curves from testing of ADF-3–based fibers (sample 1, Table 1). The curves represent analysis performed on seven different fiber fragments, each 1/2 inch in length.

mains into β sheets (*29*). The tenacity values of rc–spider silk fibers was lower than that of native dragline silk; however, from this and other studies (*29*), comparison of the effects of draw on diameter and tensile strength suggests that it should be possible to generate fibers similar to native dragline silk with further optimization of the spinning process.

A decrease in the diameter of the spun fiber with higher draw correlated with increased birefringence (Fig. 6). Upon drawing, birefringence in silks is positively correlated with molecular orientation, resulting in an increase in the proportion of the β-sheet crystalline areas and amorphous domains (*36*, *37*). A transition of birefringence was shown between the ADF-3 His and ADF-3 fibers (Fig. 6, B and D). ADF-3 His fibers were brittle, whereas ADF-3 fibers demonstrated appreciable mechanical properties.

Fibers observed microscopically after mechanical testing were generally uniform with distinct areas of elongation. These elongated areas showed a 12% diameter decrease and were not associated with the break point (Fig. 6E). This phenomenon resembles the deformation behavior of polyethylenes in which chains are pulled into the "elongated" area and a "necking" is propagated along the fiber (*38*).

Scanning electron microscopy (SEM) verified the ability to spin solid core fibers using our aqueous process. A scanning micrograph of an as-spun ADF-3 fiber stored at 50% humidity is shown in Fig. 7. The figure shows the cylindrical, smooth surface of the spun ADF-3 fiber, as well as the solid interior core of the fiber.

Spiders have perfected the process by which the non-Newtonian silk fluid/dope is transformed into fine silk filaments at ambient temperature and with low energy expenditure (*37*, *39*) by using shear-sensitive liquid crystalline silk secretions, high protein concentration, and low spinning speeds (*7*). It was previously thought that the silk protein sequence would be the primary factor determining fiber properties. We spun fibers from one (ADF-3) of the two proteins present in dragline silk with a molecular mass of 60 kD (*1*) and mechanical properties approaching those of native spider dragline silk. This result raises the question of the contribution of the second protein, ADF-4 or MaSpI, to the silk's fiber properties.

Conditions under which the fibers are spun and processed (for example by drawing) are critical in determining mechanical properties. Wet spinning of rc-silk as described here depends on a chemical transformation and several postspinning draw steps for achieving fiber properties presumably due to aligned microstructure (*38*). In contrast, spiders produce silks as a result of rapid physical transformation in a single processing step in parallel with drawing because postspinning draw is precluded (*7*, *37*, *39*). The spinning parameters allow for a modular process design resulting in fiber formation diversity starting with a common primary silk protein sequence. It is anticipated that by varying the silk primary sequences and spinning parameters, fibers with a range of specifications can be produced (*37*). These fibers could be used in a variety of applications: for example, as very fine monofilament sutures in microsurgery or in uses requiring a high level of energy absorption and elongation similar to that provided by Nylon (*37*, *40*). In contrast to the manufacture of aramid fibers, a process that requires highly concentrated sulfuric acid, production of rc–spider silk using water as the solvent offers obvious advantages (*40*). An additional benefit is that silk will ultimately degrade in aqueous environments, providing a "green" alternative to traditional synthetic fibers (*40*).
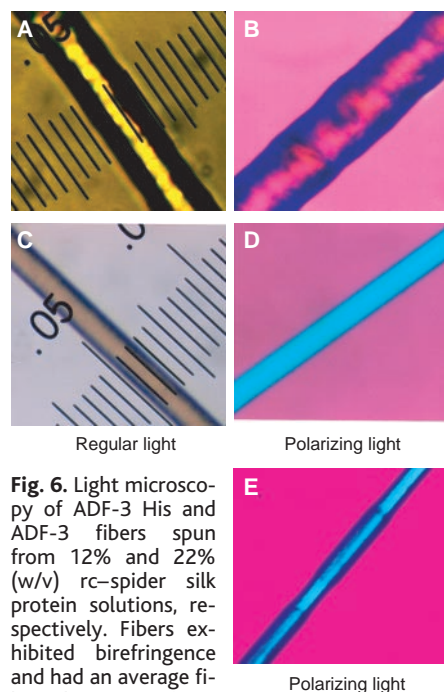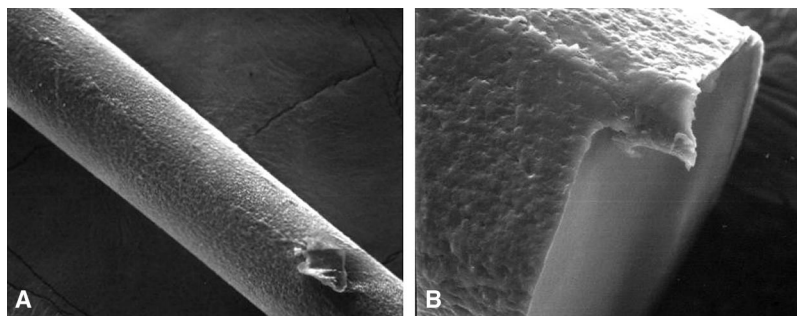

Fig. 6. Light microscopy of ADF-3 His and ADF-3 fibers spun from 12% and 22% (w/v) rc–spider silk protein solutions, respectively. Fibers exhibited birefringence and had an average fiber diameter of 20 μm. (**A** and **C**) Regular light microscopy for ADF-3 His and ADF-3 fibers, respectively. (**B** and **D**) Polarizing light microscopy with a 530-nm first-order red plate for ADF-3 His and ADF-3, respectively. (**E**) ADF-3 fiber spun from a 22% (w/v) rc–spider silk protein solution in methanol, then drawn fourfold in methanol and once in water. The fiber was observed under polarizing light with a 530-nm first-order red plate. Areas of elongation are apparent after the fiber has undergone mechanical testing.

Fig. 7. Scanning electron micrographs of an ADF-3 as-spun fiber. (**A**) Analysis of fiber surface (magnification, ×500); (**B**) analysis at a break point to examine the fiber interior core (×2000).

References and Notes

1. M. W. Denny, *J. Exp. Biol.* **65**, 483 (1976).
2. J. M. Gosline et al., *Endeavour* **10**, 38 (1986).
3. M. Hinman et al., in *Biopolymers* (Springer-Verlag, Berlin-Heidelberg, 1992), pp. 227–254.
4. F. Lucas, *Discovery* **25**, 20 (1964).
5. J. Koover, in *Ecophysiology of Spiders*, W. Nentwig, Ed. (Springer-Verlag, Berlin, Heidelberg, 1987), pp. 160–186.
6. J. Gatesy et al., *Science* **291**, 2603 (2001).
7. F. Vollrath, D. P. Knight, *Nature* **410**, 541 (2001).
8. R. W. Work, *Text. Res. J.* **46**, 485 (1976).
9. J. C. Zemlin, Technical Report No. 69-29-CM (AD684333) (U.S. Army Natick Laboratories, Natick, MA, 1968).
10. D. L. Kaplan et al., in *Silk polymers—Materials Science and Biotechnology*, D. L. Kaplan, W. W. Adams, B. L. Farmer, C. Viney, Eds. (American Chemical Society, Washington, DC, 1994), pp. 2–16.
11. P. A. Guerette, D. G. Ginzinger, B. H. F. Weber, J. M. Gosline, *Science* **272**, 112 (1996).
12. M. Xu, R. V. Lewis, *Proc. Natl. Acad. Sci. U.S.A.* **87**, 7120 (1990).
13. M. B. Hinman, R. V. Lewis, *J. Biol. Chem.* **267**, 19320 (1992).
14. M. B. Hinman, J. A. Jones, R. V. Lewis, *Trends Biotechnol.* **18**, 374 (2000).
15. C. Y. Hayashi, N. H. Shipley, R. V. Lewis, *Int. J. Biol. Macromol.* **24**, 271 (1999).
16. J. M. Gosline, P. A. Guerette, C. S. Ortlepp, K. N. Savage, *J. Exp. Biol.* **202**, 3295 (1999).
17. C. Y. Hayashi, R. V. Lewis, *Science* **287**, 1477 (2000).
18. S. R. Fahnestock, S. L. Irwin, *Appl. Microbiol. Biotechnol.* **47**, 23 (1997).
19. J. T. Prince, K. P. McGrath, C. M. DiGirolamo, D. L. Kaplan, *Biochemistry* **34**, 10879 (1995).
20. S. R. Fahnestock, L. A. Bedzyk, *Appl. Microbiol. Biotechnol.* **47**, 33 (1997).
21. R. V. Lewis, M. Hinman, S. Kothakota, M. J. Fournier, *Protein. Expr. Purif.* **7**, 400 (1996).
22. S. Arcidiacono, C. Mello, D. Kaplan, S. Cheley, H. Bayley, *Appl. Microbiol. Biotechnol.* **49**, 31 (1998).
23. S. R. Fahnestock, Z. Yao, L. A. Bedzyk, *Rev. Mol. Biotechnol.* **74**, 105 (2000).
24. J. Scheller, K.-H. Guhrs, F. Grosse, U. Conrad, *Nature Biotechnol.* **19**, 573 (2001).
25. R. L. Lock, U.S. Patent 5,252,285 (1993).
26. O. Liivak et al., *Macromolecules* **31**, 2947 (1998).
27. K. A. Trabbic, P. Yager, *Macromolecules* **31**, 462 (1998).
28. A. Seidel et al., *Macromolecules* **31**, 6733 (1998).
29. A. Seidel et al., *Macromolecules* **33**, 775 (2000).
30. S. R. Fahnestock, International Patent Application, Publication No. WO 94/29450 (1994).
31. J. P. O'Brien et al., *Adv. Mater.* **10**, 1185 (1998).
32. Complete experimental protocols and figures are available on *Science* Online at www.sciencemag.org/cgi/content/full/295/5554/472/DC1.
33. G. C. Candelas, C. Arroyo, C. Carrasco, R. Dompenciel, *Dev. Biol.* **140**, 215 (1990).
34. P. M. Lizardi, V. Mahdavi, D. Shields, G. C. Candelas, *Proc. Natl. Acad. Sci. U.S.A.* **76**, 6211 (1979).
35. Fiber spinning. Recombinant–spider silk fibers were wet spun into a coagulation bath containing methanol and water. A 5-μl sample of spin solution (10 to 28%) was injected into a small volume of methanol at various concentrations. The ability of the spin solution to coagulate, as well as the speed of coagulation, was considered in choosing the appropriate methanol concentration. The "prototype spinning apparatus" for rc–spider silk fiber production was a Harvard Apparatus Infusion/Withdrawal Pump (Harvard Instruments, Natick, MA) equipped with a specialized microspinner (cavity volume 0.5 ml, 5 mm internal diameter), and a 6-cm-long, 0.005-inch (0.125 mm internal diameter) PEEK HPLC tubing (Sigma-Aldrich) was used as a spinneret. As little as 25 μl of dope rc–spider silk solution could be spun. Spin solutions were extruded into the coagulation bath at a pump speed of 2 to 10 μl/min. Single-drawn fibers were hand-drawn while in the methanol/water coagulation bath. Double-drawn fibers were drawn first in the bath as described above, followed by drawing in water at ambient temperature. The fiber was held constrained at both ends while being moved to the water bath as well as while being air-dried.
36. R. W. Work, *Text. Res. J.* **47**, 650 (1977).
37. C. Viney, in *Structural Biological Materials: Design and Structure-Property Relationships*, M. Elices, Ed. (American Chemical Society, Washington, DC, 2000), vol. 10, pp. 295–333.
38. Y. Termonia, in *Structural Biological Materials: Design and Structure-Property Relationships*, M. Elices, Ed. (American Chemical Society, Washington, DC, 2000), vol. 10, pp. 271–291.
39. C. Viney et al., in *Silk Polymers—Materials Science and Biotechnology*, D. L. Kaplan, W. W. Adams, B. L. Farmer, C. Viney, Eds. (American Chemical Society, Washington, DC, 1994), pp. 120–136.
40. Y. Termonia, in *Structural Biological Materials: Design and Structure-Property Relationships*, M. Elices, Ed. (American Chemical Society, Washington, DC, 2000), vol. 10, pp. 337–349.
41. We thank R. Lewis and J. M Gosline for providing cDNAs, and S. Islam for critical evaluation of the fiber mechanical testing data; J. Turner for valuable discussions; R. Keyston for help during the early stages of this work; and members of our laboratory for their support. We also thank D. Ziegler (Natick Soldier Center) for the SEM micrographs and S. Fossey, C. Mello, R. Segars, and J. Herbert (Natick Soldier Center) for valuable discussions. This work was supported by the Defense Industry Research program of the Canadian Department of Natural Defense (Val Cartier, PQ).

28 August 2001; accepted 11 December 2001

Positive Mass Balance of the Ross Ice Streams, West Antarctica

Ian Joughin[1]* and Slawek Tulaczyk[2]*

We have used ice-flow velocity measurements from synthetic aperture radar to reassess the mass balance of the Ross Ice Streams, West Antarctica. We find strong evidence for ice-sheet growth (+26.8 gigatons per year), in contrast to earlier estimates indicating a mass deficit (−20.9 gigatons per year). Average thickening is equal to ~25% of the accumulation rate, with most of this growth occurring on Ice Stream C. Whillans Ice Stream, which was thought to have a significantly negative mass balance, is close to balance, reflecting its continuing slowdown. The overall positive mass balance may signal an end to the Holocene retreat of these ice streams.

Over the past several decades there has been concern that the marine-based West Antarctic Ice Sheet might collapse within the next several centuries, raising sea level by 5 to 6 m (*1*). Underlain by a thick layer of marine sediments, this ice sheet has exhibited considerable change in flow over the last millennium, particularly along the Siple Coast in the Ross Sea Sector (*2*), and since the last glacial maximum, the grounding line (the point where the ice sheet loses contact with its bed and begins to float) has retreated nearly 1300 km along the western side of the Ross Embayment. The chronology established for this retreat suggests mean grounding-line migration rates of 120 m/year (*3*). Although other processes might intervene, extrapolation of these rates has been used to predict a 4000-year lifetime for the West Antarctic Ice Sheet (*4*). Although this is a much longer period than earlier estimates (*5*) that predict a collapse over a few centuries, it does imply a sea-level rise of 12.5 to 15 cm per century.

Hypotheses of continued grounding-line retreat and possible collapse have been supported by an estimate of −20.9 ± 13.7 Gton/year (*6, 7*) for the mass balance of the Ross Ice Streams (A to F) (Fig. 1). This negative value by Shabtaie and Bentley (S&B) (*6*) implies that ice discharge (loss) exceeds accumulation by ~25%, causing the ice sheet to thin and the grounding line to retreat. Much of this imbalance has been attributed to Whillans Ice Stream (formerly known as Ice Stream B), but negative imbalances were also found for the other Ross Ice Streams, with the exception of Ice Stream C, which stagnated 150 years ago (*8*). More recent analyses (*9*) based on similar data have estimated comparable negative imbalances on Whillans Ice Stream.

The ice-discharge estimates in earlier studies relied on relatively sparse in situ measurements of ice-flow velocity (*10*). For some ice streams, the S&B discharge estimates were based on only one or two velocity measurements (*6*). We used spatially dense estimates of ice-flow velocity (Fig. 1) afforded by Interferometric Synthetic Aperture Radar

[1]Jet Propulsion Laboratory, California Institute of Technology, Mailstop 300-235, 4800 Oak Grove Drive, Pasadena, CA 91109, USA. [2]Department of Earth Sciences, A208 Earth and Marine Sciences Building, University of California, Santa Cruz, Santa Cruz, CA 95064, USA.

*E-mail: ian@radar-sci.jpl.nasa.gov, tulaczyk@es.ucsc.edu